Optimal design process of crossflow Banki turbines: Literature review and novel expeditious equations

Ocean Engineering 257 (2022) 111582

Contents lists available at ScienceDirect

Ocean Engineering

journal homepage: www.elsevier.com/locate/oceaneng

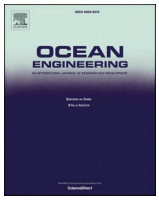

Optimal design process of crossflow Banki turbines: Literature review and novel expeditious equations

Emanuele Quaranta [a,*], Jean Pierre Perrier [b], Roberto Revelli [b]

[a] European Commission Joint Research Centre, Ispra, Italy
[b] Politecnico di Torino, Torino, Italy

ARTICLE INFO

Keywords:
Aqueducts
Banki
Crossflow
Hydropower
Ossberger
Turbine

ABSTRACT

The Banki turbine is a crossflow turbine suitable for sites with heads below 200 m and flow rates below 10 m^3/s, with maximum efficiency around 80%. Its flexible operation and easy manufacturing make it a suitable hydropower technology for different geographic areas and hydraulic contexts. However, the design procedure proposed in literature is not complete and it is quite fragmented. It lacks of effective equations to select the optimal number of blades, the optimal tip speed ratio, the rotational speed and a preliminary cost estimate. Information on runner material and blade thickness is also fragmented. In this paper, the traditional design procedures are reviewed, and a new and more complete one is proposed to overcome the above-mentioned gaps, providing new expeditious equations and data to be used in practical applications. The new equations are obtained by elaborating and generalizing literature and industrial data, presenting them in a dimensionless form. The current share of Banki turbines and their future developments and opportunities are also discussed.

1. Introduction

Hydropower is a renewable energy source, and it accounts for 16% of the global electricity generation, with an installed power capacity of 1330 GW in 2021 (International Energy Agency, 2021). Hydropower harnesses the energy of water to generate mechanical energy through the rotation of an hydraulic turbine. The mechanical energy is converted into electricity through an electric generator driven by the rotating turbine. Hydraulic turbines can be of different types: reaction turbines (e.g., Francis, Kaplan, Deriaz) mainly use the water pressure, impulse turbines (e.g., Pelton, Turgo, Banki) mainly use the water kinetic energy, and gravity turbines (e.g., water wheels and Archimedes screws) mainly use the weight of water (Okot, 2013; Quaranta and Revelli, 2018).

The Banki turbine, also known as Ossberger or Michel turbine, is the topic of the present study. It is composed of two main components, usually made of stainless steel (pers. comm. Italperfo s.r.l., 2021, pers. comm. Ossberger GmbH-Co, 2021, see details in *Materials*): a nozzle to control the flow entering the runner blades and the runner to extract the power from the flow (Adhikari, 2016). The runner is placed in a casing at atmospheric pressure, and it is connected to the generator through a shaft. A draft tube can be installed to exploit the residual head downstream and for in-conduit operation (e.g., aqueducts, Sinagra et al., 2020). The Banki turbine is a crossflow turbine because the water flow acts twice on the blades: the water jet interacts with the blades when they are near the nozzle (first stage), then the water jet flows from their outlet to the inlet of the same blades when they have reached the opposite side (second stage), as depicted in Fig. 1 (Adhikari, 2016).

The energy exchanged is typically 70–90% and 10–30% in the first and second stage, respectively. De Andrade et al. (2011) carried out computational fluid dynamic (CFD) simulations with the aim of highlighting the contribution of the two stages: they showed that 68.5% of energy is generated in the first stage, while in the second stage the remaining 31.5%. Adhikari and Wood (2018) demonstrated that the difference between the two stages is reduced as the flow rate increases: by doubling the flow rate, the percentages of energy produced in the first and second stages change from 88%-12% to 78%–22%, respectively. Woldermariam and Lemu (2019) found that the second stage contributes from 36.4% to 53.7%.

Full scale Banki turbines operate for a wide range of heads, from a few meters up to 200 m, and with low flow rates, from about 0.5 m^3/s to 10 m^3/s (Adhikari, 2016). The power capacity is between 10 kW and 1000 kW (Fig. 2). Recently developed designs, especially for enclosed pipes, can operate at heads >150 m and flows below 0.2 m^3/s (Picone

* Corresponding author.,
E-mail addresses: emanuele.quaranta@ec.europa.eu, quarantaemanuele@yahoo.it (E. Quaranta), jeanprperrier@gmail.com (J.P. Perrier), roberto.revelli@polito.it (R. Revelli).

https://doi.org/10.1016/j.oceaneng.2022.111582
Received 24 January 2022; Received in revised form 4 April 2022; Accepted 16 May 2022
Available online 29 May 2022

Nomenclature

A	Area [m^2]
B	Runner width [m]
b	Nozzle width [m]
C	Loss coefficient (coefficient accounting for nozzle roughness) [-]
c_v	Outflow coefficient [-]
D_1	Runner outer diameter [m]
D_2	Runner inner diameter [m]
g	Acceleration of gravity [m/s^2]
H	Gross head [m]
H_n	Net head [m]
L_c	Length of the blades [m]
N	Runner rotational speed [rpm]
N_b	Number of blades [-]
N_s	Characteristic speed [-]
P	Power [kW]
Q	Flow rate [m^3/s]
Q'	Specific flow rate [-]
R_1	Runner outer radius [m]
R_2	Runner inner radius [m]
s	Depth of the jet [m]
S_0	Nozzle throat [m]
S_c	Distance between the centre of two adjacent blades [m]
SR	Tip speed ratio [-]
t	Distance between the tip of two adjacent blades [m]
t_b	Thickness of blades [m]
U	Runner peripheral velocity [m/s]
V	Absolute velocity of water [m/s]
W	Relative flow velocity [m/s]
α	Angle of attack [deg]
β_1	Inlet flow angle [deg]
β_2	Outlet flow angle [deg]
δ	Central angle of the blade [deg]
η	Efficiency [-]
λ	Nozzle entry arc angle [deg]
ρ	Water density [kg/m^3]
ρ_b	Blade curvature radius [m]
σ	Blending strength [MPa]
ψ	Loss coefficient (coefficient accounting for blade roughness) [-]
ω	Runner angular velocity [rad/s]

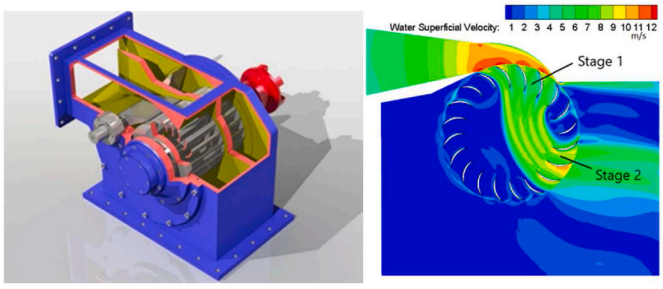

Fig. 1. Working behaviour of the Banki turbine.

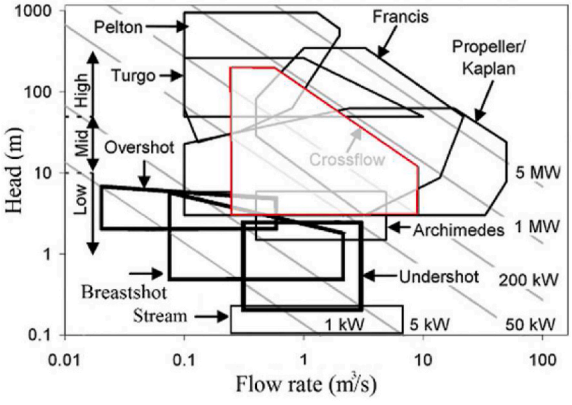

Fig. 2. Operating range of the Banki turbines, adapted from Quaranta and Revelli (2018).

et al., 2021). The characteristic speed N_s, defined in Eq. (1), ranges from 60 to 200 (Restrepo, 2014):

$$N_s = \frac{NP_{out}^{1/2}}{H_n^{1.25}} \quad [-] \tag{1}$$

where N = runner rotational speed [rpm], P_{out} = installed power [kW], H_n = net head [m].

The maximum hydraulic efficiency is approximately 80% (Anand et al., 2021), and it is defined as the ratio of power output to power input:

$$\eta = \frac{P_{out}}{P_{in}} = \frac{M\omega}{\rho g H_n Q} \quad [-] \tag{2}$$

where M = shaft torque [Nm], ω = runner angular velocity [rad/s], ρ = water density [kg/m^3], g = acceleration of gravity [9.81 m/s^2], Q = flow rate [m^3/s]. The net head H_n can be approximately calculated as 0.94 H where H is the gross head (Nasir, 2013).

The main parameters that characterize the nozzle are depicted in Fig. 3 (Sammartano et al., 2013): the nozzle width b, the nozzle throat (or depth) S_0 and the angle of attack α, namely the angle between the direction of water velocity and the tangent line to runner inlet. The nozzle profile has a particular shape to allow the flow to enter the runner always with the same angle α. The runner is characterized by the width B, the outer and inner diameters D_1 and D_2, the entry angle arc λ and the number of blades N_b, that are characterized by the radius ρ_b, the central angle δ and the inlet and outlet flow angle β_1 and β_2. β_1 and β_2 are the angles between the tangent of the blade at the blade tip and the tangent to the external and internal circumference of the runner, respectively.

1.1. Flow rate regulation

The flow rate regulation system is depicted in Fig. 4 (Adhikari and Wood, 2018). It allows to open the turbine for one third, two thirds or three thirds, making the machine flexible towards the seasonality of the flow rates. A moving component further allows to change the flow passage area in the nozzle, for a fixed width opening (Adhikari and Wood, 2018), and it can be either a slider or a guide vane. The guide vane splits the flow in two, that undergoes a deceleration and a change in the flow trajectory, resulting in an irregular velocity profile to the runner inlet and a deviation from the optimal direction. This leads to an efficiency reduction. The slider, on the other hand, is a metal plate of semi-circular section that, sliding tangentially to the runner, acts on the amplitude of the entry arc angle. The water flow enters directly into the runner without undergoing a deceleration and without energy dissipation in the nozzle (Sinagra et al., 2014). Adhikari and Wood (2018)

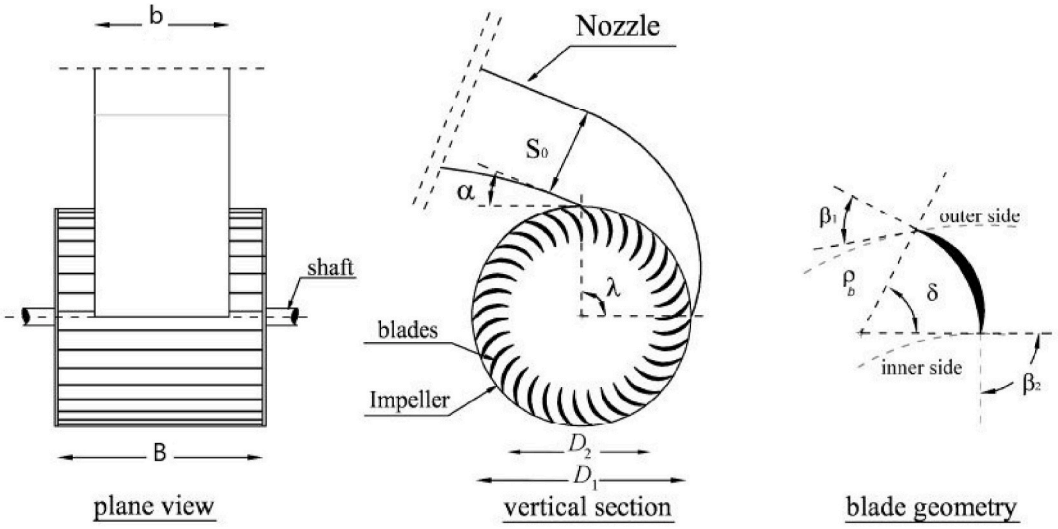

Fig. 3. Dimensions of a Banki turbine.

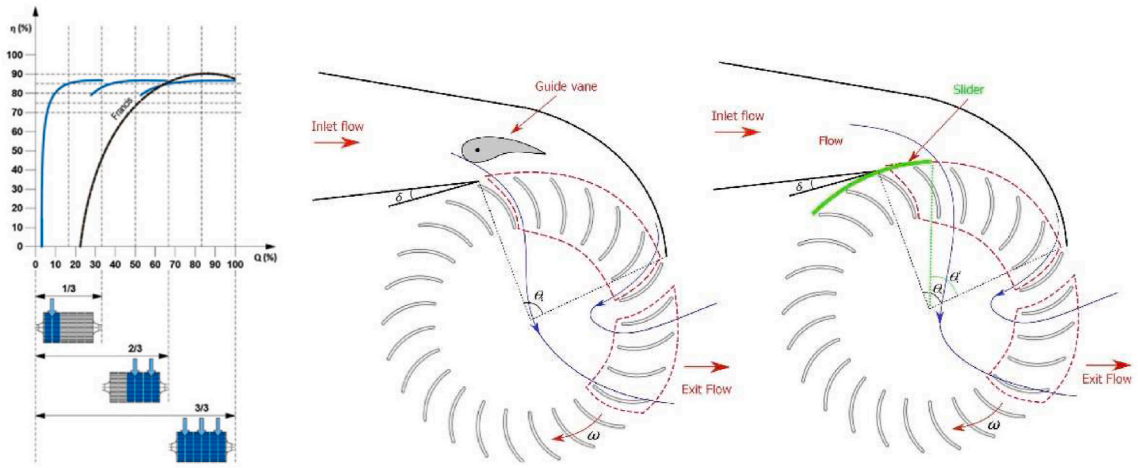

Fig. 4. Flow regulation of a Banki turbine.

achieved the same maximum efficiency (88%) with the guide vane and the slider, but with the slider the turbine could maintain a high efficiency up to lower flow rates.

Mehr et al. (2019) and Sinagra et al. (2014) have highlighted the ability of the turbine to work well with flow rates as low as 16%–20% of the maximum flow rate, and this quality is linked to the regulation systems. The 16% can be reached by opening one third of the width of the turbine and then halving the flow rate by the nozzle. This has been confirmed in a real hydropower plant described in Cesoniene et al. (2020).

1.2. Why the Banki turbine?

In the recent years, new market, technological and social needs require hydropower to be more flexible, less environmental impactful and more cost effective, with new developments in existing infrastructures and in remote areas (Quaranta et al., 2020; International Energy Agency, 2021). Within this context, the Banki turbine represents an interesting technology and with new development opportunities, especially thanks to its simplicity in construction, flow rate/power regulation capacity and possibility to be installed both in traditional hydropower plants and in existing infrastructures, e.g. in aqueducts. In the former case, the plant has the typical configuration with inlet gate, penstock and turbine. In the second case, the Banki turbine is used as PRS (Pressure Reducing System): the turbine is installed in the pipeline with the dual function of dissipating pressures and generating energy. Additional applications of the Banki turbines are discussed in Appendix 4.

The manufacture of Banki turbines is quite simple compared to other types of turbines and can also be made in an artisanal way. The Banki turbines are basically made up of two circular rims joined together by welded blades. Therefore, the Banki turbine has great potential in rural areas, isolated and difficult to reach, in Non-Interconnected Zones and in low-income countries, but also in more industrialized countries (Ceballos et al., 2017). Some example are in Camerun (Ho-Yan e Lubitz, 2011), Tanzania (Mtalo et al., 2010), Pakistan (Chattha et al., 2014; Khan and Badshah, 2014), Bangladesh (Das et al., 2013), Nepal (Acharya et al., 2019), Myanmar (Win et al., 2016), Colombia (Durali, 1976). Fig. 5 depicts the distribution of the studies collected in the present manuscript. Das et al. (2013) compared a Banki turbine with a micro-Kaplan turbine of the same power and claimed that the Banki costs up to 7 times less in Bangladesh. 26 Banki turbines have been designed for 16 small hydropower plants in Bulgaria, with heads ranging from 22 m to 142 m and power up to 500 kW (Obretenov and Tsalov, 2021), while 6% of installed turbines in Saxony are Banki type (Spänhoff, 2014). In the European Union + UK (EU28), according to

Fig. 5. Geographic distribution of the collected studies.

Voith Hydro database (pers. comm. of Markus Wirth), 24 Banki turbines are installed with a total power of 10.4 MW and maximum head 170 m.

Compared to the Francis turbine, the Banki turbine is able to guarantee an almost flat efficiency curve for a wider range of flow rates, although the maximum efficiency is generally lower (5–10 percentage points).

The life-span ranges from 40 to 50 years. Throughout its life, the Banki turbine does not require excessive maintenance, and this is also helped by the fact that the flow, passing through the runner, favors the self-cleaning capacity of the machine by continuously removing the sediments (pers. comm. of Ossberger GmbH-Co, 2021). In addition, as reported by Durali (1976) and in the technical specifications of the turbines produced by CINK Hydro-energy, the bearings are not in direct contact with the flow, but are protected by coatings, and can be easily lubricated and controlled, thus facilitating maintenance and increasing durability. In particular, the Ossberger company designs the bearings in order to guarantee a minimum operating life of 100 thousand hours, that is, more than 10 years (pers. comm. of Alberto Santolin, 2021). Finally, the study conducted by Adhikari et al. (2016) on a 7 kW turbine, showed that cavitation was found only in the second stage, minimizing cavitation erosion.

1.3. Design challenges and scope of the work

In Anand et al. (2021) the most recent review on the Banki turbine has been presented, with focus on its hydraulic behaviour and performance. The scientific challenges and gaps were also highlighted. A dataset collection of Banki turbines from literature was included, with the main geometric characteristics. Therefore, the reader interested in better understanding the Banki turbine behaviour and the literature research that has been carried out until year 2021 can refer to Anand et al. (2021). However, since a comprehensive design methodology for the Banki turbine has not been presented yet and it is not clear how to select some design parameters, the design gaps that are addressed in this study are the following.

1) Rotational speed N: it can be generally estimated with an iterative process and choosing a certain value of D/B (diameter to width ratio of the runner). However, there is no systematic information on the optimal D/B value, and there are not expeditious tools able to easily estimate N for preliminary purposes. The only available equation to estimate the rotational speed is a function of the characteristic speed (Eq. (7)), but it does not effectively work over the entire range of operating conditions of the Banki turbine, since it is not dimensionless. This is also a lack encountered in similar equations for Francis and Kaplan turbines (Quaranta, 2019).
2) Speed ratio $SR = U/V_U$: this is defined as the ratio of U, the blade tangential speed, to V_u, the inflow water velocity existing the nozzle and projected along the U direction. The theoretical optimal value is $SR_{th} = 1/2$, by applying the velocity triangle theory and finding the maximum power (Desai and Aziz, 1994; Das et al., 2013):

$$SR_{th} = \frac{U}{V_u} = \frac{U}{V\cos\alpha} = \frac{1}{2}\,[-] \tag{3}$$

with:

$$V_U = c_v\sqrt{2gH_n}\cdot\cos\alpha\ \left[\frac{\mathrm{m}}{\mathrm{s}}\right] \tag{4}$$

$$U = \omega\frac{D_1}{2} = \frac{2\pi N}{60}\cdot\frac{D_1}{2} = \frac{\pi N D_1}{60}\ \left[\frac{\mathrm{m}}{\mathrm{s}}\right] \tag{5}$$

where α is the angle of attack, c_v is the outflow coefficient, H_n is the net head [m], N is the rotational speed [rpm], ω is the rotational speed [rad/s] and D_1 is the outer diameter [m]. c_v is as a function of U/V_u and impeller inlet pressure (see Sammartano et al., 2016), and it can be assumed $c_v = 0.98$ when the inlet is at atmospheric pressure.

Experimental studies show that the optimal SR is generally higher than the theoretical one SR_{th}, but there are not practical suggestions on which SR value should be selected for the design.
3) Number of blades N_b: different equations have been proposed in literature, but they exhibit some limitations: Khan and Badshah (2014) and Sammartano et al. (2016) are only valid in the investigated range, while Verhaart (1983) simply identifies the minimum number of blades to satisfy structural constraints and manufacture issues. Mockmore and Merryfield (1949) equation is an old empirical

equation only valid within that study. These equations are better described in the *Results* section.

4) Blade thickness: this parameter has been analysed in some papers (Verhaart, 1983; Khan and Badshah, 2014), but a complete methodology has not been proposed within the overall dimensioning process of a Banki turbine, and the related information has never been discussed in a systematic way. It must be noted that the blade thickness is not the only design parameter of blade design, as also the profile and the thickness variation along the blade are relevant (Sinagra et al., 2021).
5) The shape ratio D_1/b (outer runner diameter to the nozzle width) has never been adequately discussed, except in Khosrowpanah et al. (1988). In most of the studies, $b = B$ (B=runner width), so that $D_1/b = D_1/B$. In other cases, $B > b$ (see Appendix 3) to improve the efficiency, where b is estimated from the continuity of the discharged flow.

Additional issues not appropriately investigated in the literature are here addressed. Cost data were provided from hydropower companies and some Italian projects found on websites of local authorities. A section on the used materials is also provided thanks to information provided by companies, while the environmental performance (fish, sediment management, and cavitation problems) is described based on scientific literature data, writing a comprehensive section that aims at summarizing the fragmented literature information.

2. Review of design methodologies

In this section, the design methodologies available in literature are discussed. The first methodology was discussed in Mockmore and Merryfield (1949) and then adopted and improved by other authors (see next paragraph). Over the last decades, more advanced methodologies, e.g. those developed by Sammartano et al. (2013, 2016), optimize and complete the traditional methodology by proposing more complete equations, with optimized design parameters, especially for the blade angles and for the distributor profile. Methodologies based on iterative processes and on more design steps have been also introduced, that usually include Computational Fluid Dynamic (CFD) simulations (e.g., Hannachi et al., 2021; Mehr et al., 2019). However, these methodologies do not always solve the above mentioned gaps in an expeditious way, do not often provide generalizable results and are limited within the range of the investigated study.

Therefore, literature was surveyed, and relevant examples and data were compiled to assist the development of a new methodology, that was thus conceived to fill these gaps (most of the data are presented in Appendix 1, 2 and 3). The proposed methodology starts from the available equations or suggestions and improves the selection of the input parameters based on a critical review of literature data, expressing these input parameters as a function of other parameters when possible. In the following chapters some of the existing equations are improved, while new equations are introduced, replacing/complementing the old ones, e.g. those to estimate N_b, N and SR. These new equations were achieved considering only the studies where more values of these parameters were tested, so that the optimized ones could be selected and used in our analysis. Practical considerations on materials, costs, blade thickness t_b and D_1/b are also discussed.

2.1. Original methodology

Mockmore and Merryfield (1949) proposed the first design methodology, based on a jet impinging on one blade at time, and equipped with a guide vane for the flow regulation. This methodology was later adopted by other studies, e.g. Nasir (2013), Chattha et al. (2014), Achebe et al. (2020), Das et al. (2013), Acharya et al. (2019), Win et al. (2016), Mehr et al. (2019).

The maximum achievable efficiency η, from a theoretical point of view is (Mockmore and Merryfield, 1949):

$$\eta = \frac{C^2 \cdot (1 + \Psi) \cdot cos^2 \alpha}{2} \quad [-] \tag{6}$$

where C and Ψ are loss coefficients that are generally set to 0.98 in the engineering practice (Mockmore and Merryfield, 1949). The angle of attack α typically ranges from 16° (Michell, 1903; Mockmore and Merryfield, 1949; Durali, 1976; Khosrowpanah et al., 1988) to 24° (Fiuzat and Akerkar, 1989), and in some cases it is 22° (Desai and Aziz, 1994; Totapally and Aziz, 1994).

By assuming $N_s = 513/H_n^{0.505}$ (Desai e Aziz, 1994; Penche, 1998; San and Nyi, 2018), Eq. (1) gives:

$$N = \frac{513 \cdot H_n^{0.745}}{\sqrt{P_{out}}} \ [\text{rpm}] \tag{7}$$

The diameter can be estimated from the speed ratio, i.e. Eqs. (3)–(5):

$$D_1 = \frac{82.9 \cdot SR_{th} \cdot \cos \alpha \cdot \sqrt{H_n}}{N} \ [\text{m}] \tag{8}$$

The internal diameter D_2 can be estimated as $x\ D_1$, with x ranging from 0.65 to 0.68, in particular it was 0.65 in Sinagra et al. (2014) and Nasir (2013), 0.66 in Mockmore and Merryfield (1949) and Chattha et al. (2014), 0.67 in Adhikari (2016), 0.68 in Durali (1976), Khosrowpanah et al. (1988), Fiuzat and Akerkar (1989), Totapally and Aziz (1994) and Desai and Aziz (1994). In few cases it is 0.75 (Anand et al., 2021).

The inflow angle is:

$$\tan \beta_1 = 2 \tan \alpha \tag{9}$$

The outflow angle is instead generally set to $\beta_2 = 90°$ (Fig. 3), e.g., Mockmore and Merryfield (1949), Durali (1976), Fiuzat and Akerkar (1989), Khosrowpanah et al. (1988), Desai and Aziz (1994), Adhikari and Wood (2018) and Nasir (2013).

The depth of the water jet just upstream of the balde tip s was suggested to be:

$$s = k \cdot D_1 \ [\text{m}] \tag{10}$$

with k = 0.075–0.1 (Mockmore and Merryfield, 1949), with a typical adopted value of k = 0.087 (Nasir, 2013; Mockmore and Merryfield, 1949).

Therefore, the distance between two blades t is:

$$t = \frac{s}{\sin \beta_1} \ [\text{m}] \tag{11}$$

Nasir (2013) suggested the following equation to estimate t, with $\alpha = 16°$, $\beta_1 = 30°$ e $k = 0.087$:

$$t = 0.174 D_1 \ [\text{m}] \tag{12}$$

The width of the nozzle can be calculated from the continuity equation:

$$Q = V \cdot s \cdot b \xrightarrow{yields} b = 0.077 \frac{N \cdot Q}{H_n \cdot \cos \alpha} \ [\text{m}] \tag{13}$$

The curvature radius ρ_b of the blade profile is a function of the blade angles and inner and outer radius, R_1 and R_2, respectively:

$$\rho_b = \frac{\left[R_1^{\,2} - R_2^{\,2}\right]}{2(R_1 \cos \beta_1 + R_2 \cos \beta_2)} \ [\text{m}] \tag{14}$$

The angle at the centre of the blade δ is:

$$\tan \frac{\delta}{2} = \frac{\cos \beta_1 - \frac{R_2}{R_1} \cos \beta_2}{\sin \beta_1 + \frac{R_2}{R_1} \text{sen} \beta_2} \quad [-] \tag{15}$$

The product $\rho_b \delta$ gives the blade length L_c (m).

2.2. Recent methodologies

The modern design methods have improved the original design, especially the design of the blades and the nozzle arc, considering that more blades interact with the water jet along the entry arc angle λ (Fig. 6, from Sammartano et al., 2013). CFD simulations are often carried out to further optimize the design parameters (Mehr et al., 2019). Most of these methodologies have been developed for applications in closed pipes, e.g. in aqueducts (Sinagra et al., 2020, 2021; Hannachi et al., 2021; Sammartano et al., 2017).

The angle of attack α is generally set at 22° (and the nozzle profile designed to maintain α along the nozzle arc), and the angle β_1 is calculated as in Sammartano et al. (2013):

$$\beta_1 = \tan^{-1}\left(\frac{V \sin\alpha}{V\cos\alpha - \omega \cdot D_1/2}\right) \text{ [deg]} \tag{16}$$

At the optimal theoretical speed ratio (Eq. (3)), Eq. (16) becomes Eq. (9). The outflow angle is again generally set to $\beta_2 = 90°$. The thickness profile along the blade can be calculated as suggested in Sinagra et al. (2021).

The diameter is determined by Eq. (8). The width of the distributor can be calculated from the mass conservation equation:

$$Q = b\ V \sin\alpha \cdot \lambda \cdot \frac{D_1}{2} = S_0\ V\ b \ \left[\frac{\text{m}^3}{\text{s}}\right] \tag{17}$$

where λ is the entry arc angle, typically 90° (Anand et al., 2021), and S_0 is the nozzle throat depth [m] at $\theta = 90°$, i.e. at the runner top (measured in the direction of the runner diameter) (Fig. 6). From Eq. (17), the width b can be calculated and then the depth S_0. The difference from the oldest methodology is that here λ is fixed, and the nozzle dimensions are calculated, while in Mockmore and Merryfield (1949) S_0 is firstly empirically calculated (Eq. (10)). The velocity V in Eq. (17) depends on the net head and on the nozzle coefficient c_v (Eq. (4)): a more realistic value of c_v was proposed in Sammartano et al. (2016) as a function of U/V_u and when the impeller inlet is not at atmospheric pressure. However, the diameter D_1 depends on the rotational speed N, for which no expeditious equations haven been proposed, so that it is generally chosen iteratively to achieve a desired aspect ratio D_1/B or D_1/b.

The distributor profile can be designed with reference to Fig. 6, and with the inlet angle α between the blades.

$$r(\theta) = K \cdot \theta + \frac{D_1}{2} \text{ [m]} \tag{18}$$

where θ is the angular position in degrees, and K is defined as:

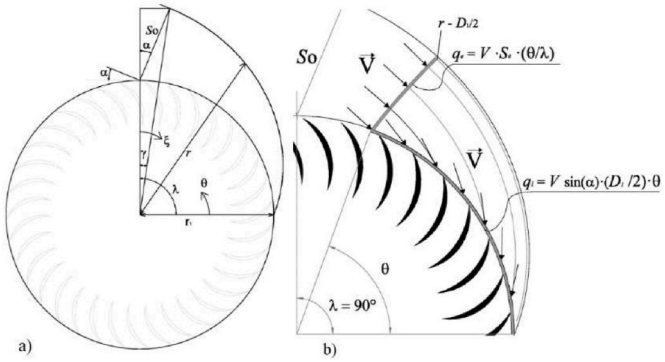

Fig. 6. Parameters of the inlet.

$$K = \frac{1}{\lambda - \gamma}\left[\frac{S_0 \cdot \cos\alpha + \frac{D_1}{2}}{\cos\gamma} - \frac{D_1}{2}\right] \text{ [m]} \tag{19}$$

$$\gamma = \tan^{-1}\left(\frac{S_0 \cdot \sin\alpha}{S_0 \cdot \cos\alpha + \frac{D_1}{2}}\right) \text{ [deg]} \tag{20}$$

Sammartano et al. (2016) proposed a diameter ratio D_2/D_1 between 0.75 and 0.80. The optimal solidity ratio L_c/S_c (ratio of length of the blades to the blade spacing) was estimated as a function of H/D_1. If the curvature radius of the blades and the angle at the centre are calculated by Eqs.(14) and (15), L_c can be calculated, as well as S_c from the optimal (known) solidity ratio L_c/S_c. S_c is a function of the number of blades. A corresponding efficiency was found for each value of L_c/S_c.

In order to optimize the efficiency, the width of the runner B can be set at a higher value with respect to b and, in general (Desai and Aziz, 1994; Achebe et al., 2020):

$$B = 1.5 \cdot b \ \text{[m]} \tag{21}$$

In Chattha et al. (2014) standardized tables were proposed with the runner dimensions as a function of head and flow. Finally, the design of the power take off (belt, pulley, generator) was discussed in Ngoma et al. (2019).

3. Proposed design methodology

3.1. Input parameters

The following input data are needed/used:

- net head H_n and flow Q
- $c_v = 0.98$ in case of atmospheric pressure inlet. See Sammartano et al. (2016) for a more realistic estimation in the other operating conditions, where c_v can reduce to 0.75–0.85.
- $\alpha = 22°$ can be selected as design angle. Perez-Rodriguez et al. (2021) showed that α between 22° and 24° optimizes the efficiency. Choi et al. (2008) showed that $\alpha = 25°$ performed better than $\alpha = 30$–$35°$.
- From Eq. (9), $\beta_1 = 39°$, or Eq. (16) could be used for a better estimation, and from literature $\beta_2 = 90°$ and $\lambda = 90°$. Choi et al. (2008), showed that $\beta_2 = 87°\sim°90$ performed better than 80° and 100°.
- The maximum efficiency is assumed equal to 80% as initial value (Anand et al., 2021).

3.2. Rotational speed, diameter, and width

The rotational speed N can be estimated by applying the methodology proposed in Quaranta (2019) for Francis and Kaplan turbines and in Quaranta and Hendrick (2020) for Deriaz turbines, in order to overcome the dimensional limitations of Eq. (7). The dimensionless rotational speed N^* and the dimensionless flow rate Q^* are defined as per Eq. (22) [1] and Eq. (23) and are plotted in Fig. 7. This methodology was applied to data collected in this study, considering the studies where the optimal rotational speed was selected among a wider range of investigated ones (Appendix 1).

$$N^* = \frac{N}{\frac{\sqrt{2gH}}{H}} \ [-] \tag{22}$$

[1] Eq. (22) is a ratio of two frequencies, where at the numerator the time is in minutes, while at the denominator it is in seconds. For practical reasons, it has been chosen not to add the factor 60 and this does not change the final result estimation.

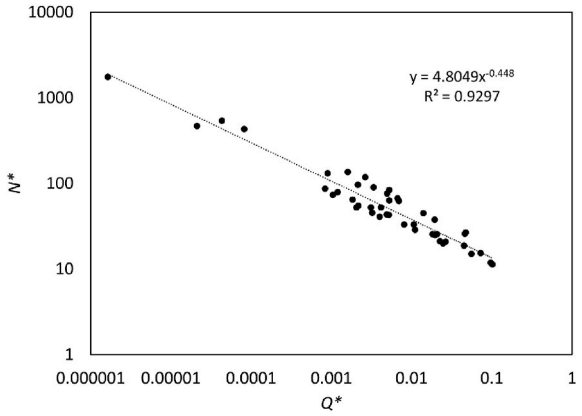

Fig. 7. Dimensionless rotational speed versus dimensionless flow rate. (Data from Appendix 1).

$$Q^* = \frac{Q}{H^2\sqrt{2gH}}\ [-] \tag{23}$$

From Fig. 7 the following expression can be deduced

$$N^* = 4.805 \cdot Q^{*-0.448}\ [-] \tag{24}$$

Fig. 8 shows the rotational speed of each study versus the estimated rotational speed (Eq. (24)). Two different trends can be identified. One for $N_s < 90$ and the other for $N_s > 90$. Therefore, results of Eq. (24) have to be multiplied by a constant, and the value of the constant is 0.93 if $N_s < 90$ and 1.35 if $N_s > 90$. The runaway speed ranges between $N_{run} = 1.8\ N$ and $N_{runaway} = 2.5\ N$ (Niyonzima, 2020; pers. comm. Ossberger GmbH-Co, 2021). In Fig. 7, there are 4 cases with a relatively low Q^*, to which correspond full scale turbines and $H_n > 10$ m.

It must be noted that the calculated value of N from Eqs.(22)–(24) is a preliminary rotational speed, and two factors should be considered:

1) when the turbine is equipped with an asyncronous generator, the rotational speed depends on the number of poles p according to $f \cdot 120/p$, where f is the grid frequency (generally, 50 or 60 Hz).
2) An adequate D_1/b ratio has to be satisfied, similarly to Pelton turbines, where an adequate ratio of runner diameter to jet diameter has to be achieved. The ratio D_1/b is recommended to range between $\frac{H^{0.85}}{21}$ and 6.25 (Ebhota and Tabakov, 2021), while it was suggested to be $\frac{D_1}{b} = \frac{cos\beta_1\sqrt{2g\eta}\ \lambda}{6Q'}$ (with $B = b$ and $Q' = Q\,D^{-2}H^{-1/2}$) in Khosrowpanah et al. (1988), with common values between 1 and 3 (Appendix 3 and Khosrowpanah et al., 1988). If the ratio D_1/b is fixed, due to local constraints, the rotational speed can be estimated from Eqs. (8) and (17).

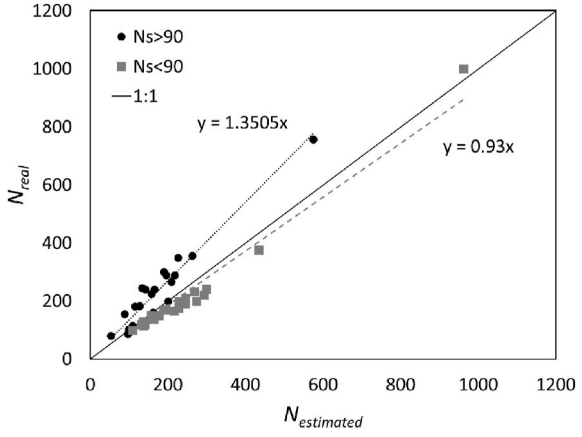

Fig. 8. Real rotational speed versus the estimated one.

The outer diameter is generally estimated using the theoretical value of the optimal speed ratio (Eq. (3) and Eq. (8)), i.e. assuming $SR_{th} = 0.5$. However, by analysing literature data, the optimal speed ratio SR_{opt} ranges from 1.1 to 1.15 the theoretical one (Appendix 2), so that an average value can be $SR_{opt}/SR_{th} = 1.13$, excluding few outliers (Fig. 9a). Furthermore, by looking at Fig. 9b, this value is correlated with the unit rotational speed $N' = N \cdot D_1 \cdot H^{-0.5}$ (Khosrowpanah et al., 1988), so that an iterative process could be implemented to determine SR_{opt} and, therefore, the optimal value of D_1. As a first tentative value, $SR_{opt}/SR_{th} = 1.13$, and D_1 can be calculated by Eq. (8) and using SR_{opt} instead of SR_{th}. N' is then calculated, and, consequently, the new SR_{opt}, until convergence, maintaining N constant. Once convergence is reached, the D_1/b value is checked and, eventually, N changed, restarting the iterative process.

The diameter D_2 can be fixed at $0.665D_1$ as average literature value. The distributor width b can be calculated from Sammartano et al. (2013), Eq. (17), and $B/b = 1.5$ to optimize the efficiency.

3.3. Blades: number, shape, and thickness

The next step consists in determining the blade design. Fig. 10 shows that the higher the number of blades, the better the hydraulic efficiency, because the water flow is more confined and is well addressed within the canal between two blades. However, when the number of blades is too high, friction losses and obstruction increase, as for water wheels (Quaranta and Revelli, 2017). Therefore, the optimal number of blades has to be estimated. Table 1 summarizes the available literature equations, and their limitations were already explained in the *Introduction* section.

By elaborating the data listed in Table 2, it is possible to obtain Fig. 11, that depicts the optimal number of blades, made dimensionless with the number of blades calculated by the equation of Mockmore and Merryfield (1949) $N_b = \frac{\pi \cdot \sin\beta_1}{k}$ (from Eqs.(10) and (11)), versus N_s. It is possible to see that the highest value of the dimensionless N_b is around $N_s = 80$, thus identifying a decreasing trend above $N_s = 80$ and an increasing trend below $N_s = 80$. Two different trends (in particular, two different coefficients) were also observed when discussing the rotational speed, above and below $N_s = 90$, a very similar value to $N_s = 80$. The optimal number of blades so calculated does not depend on the diameter, but on N_s and β_1, that means that geometrically similar runners, but of different size, require the same number of blades. This may be due to the limitations of literature data, as the considered studies tested runners with similar diameter dimensions ($D_1 = 0.30$ m, $1 < H/D_1 < 35$).

The curvature radius ρ_b of the blades can be estimated by Eq. (14), while the angle δ at the centre of the blade by Eq. (15).

Finally, the blade maximum thickness and thickness profile have to be estimated. The latter can be estimated by Sinagra et al. (2021), while the maximum thickness (at the blade centre) can be estimated by the following iterative set of equations, considering the strength of the material, the number of blades and the number of internal rims, and starting from a reasonable value of the thickness t_b (Verhaart, 1983). Table 3 shows the ratios t_b/B found in literature, that can be used as reference starting point. In Eq. (25), by assuming t_b and knowing/calculating the other variables, the blending stress σ is calculated and verified with the blending strength (see also the chapter *Materials* to select the blending strength of usual materials). The stress depends on the number of blades, and the higher N_b is, the smaller the thickness can be.

The maximum admissible strain is:

$$\sigma = 934.78 \cdot \left(\frac{9,619\rho_b}{N_b} - t_b\right) \cdot \frac{H_n \cdot B_r^2 \cdot e}{I_x}\ \left[\frac{N}{m^2}\right] \tag{25}$$

where t_b is the blade thickness [m], ρ_b is the blade curvature radius [m],

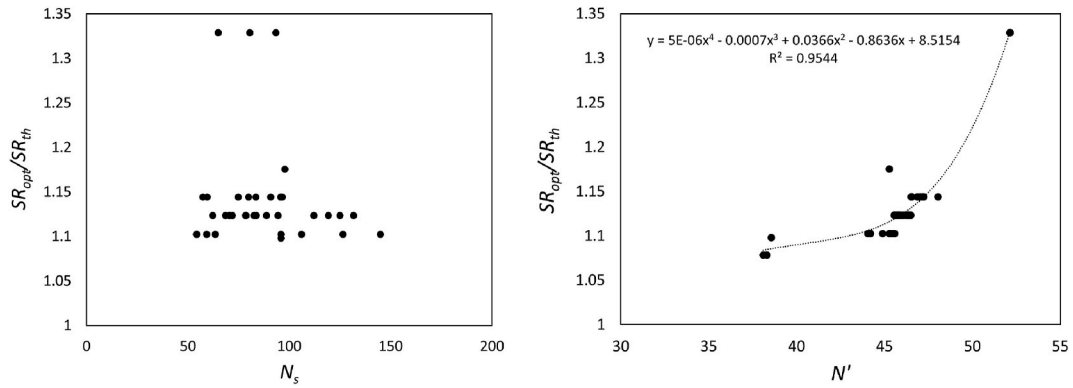

Fig. 9. Optimal tip speed ratio versus dimensionless speeds.

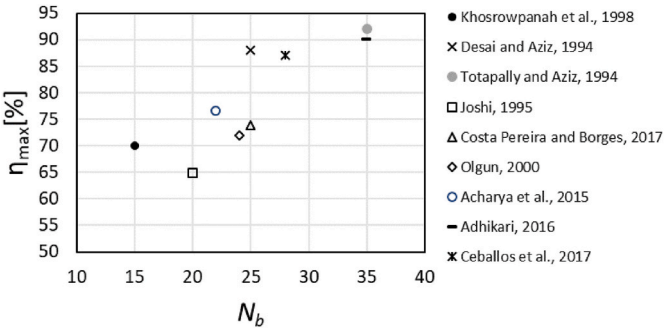

Fig. 10. Efficiency versus number of blades.

Table 1
Available equations on the number of blades N_b. t_b is blade thickness, L_c = length of the blades, S_c = distance between the blades (Sammartano et al., 2016).

Reference	Equation
Mockmore and Merryfield (1949), $k = 0.087$	$N_b = \frac{\pi \cdot \sin \beta_1}{k}$
Khan and Badshah (2014), $k_2 = 32.7$	$N_b = k_2(\pi \cdot D_1)$
Verhaart (1983)	$N_b = \frac{\pi \cdot D_1}{0.11 \cdot D_1 + t_b} + 0.5$
Sammartano et al. (2016)	$\frac{L_c}{S_c} = 10.6 \left(\frac{H_n}{D_1}\right)^{-0.266}$

N_b is the number of blades, H_n is the net head [m] and B_r is the reduced blade width, i.e. the distance between two rims [m]. The effect of the number of rims has been tested in Ebhota and Tabakov (2021), showing as an increased number of rimes is beneficial to the structural integrity of the runner, but the effects on the efficiency were not tested. I_x is the moment of inertia defined in Eq. (26):

$$I_x = \frac{10^{-4}\left(91\rho_b^4 \cdot t_b + 181\rho_b^3 \cdot t_b{}^2 + 2,019\rho_b^2 \cdot t_b^3 + 1,928\rho_b \cdot t_b^4 + 321t_b^5\right)}{(2\rho_b + t_b)} \ [\mathrm{m}^4] \tag{26}$$

where e is defined in Eq. (27):

$$e = \frac{10^{-4}\left(2,361\rho_b^2 + 10,644\rho_b \cdot t_b + 6,219t_b^2\right)}{(2\rho_b + t_b)} \ [\mathrm{m}] \tag{27}$$

The above-calculated thickness is assumed to be the maximum one, and it can be reduced from the middle of the blade to the blade side, since the maximum bending moment is at the centre of the blade. In Sinagra et al. (2021) it was also shown as the thickness at the centre of the blade depends on the angle existing between the tangents to the internal and the external surface, and the maximum efficiency depends on the profile.

San and Nyi (2018) suggested an empirical equation to calculate the shaft diameter. The shaft diameter has slight effects on the turbine

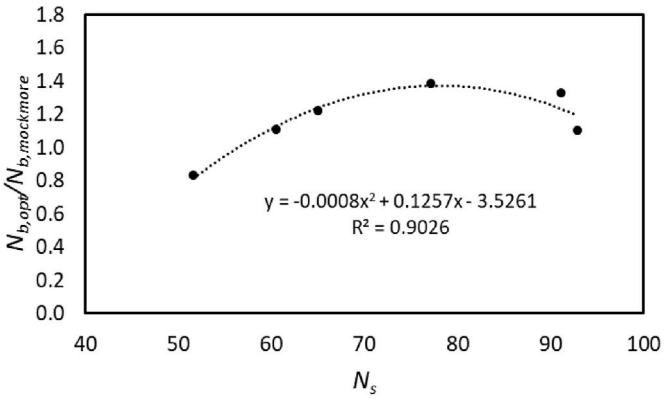

Fig. 11. Optimal number of blades (dimensionless) versus the characteristic speed.

Table 2
Optimal number of blades from literature studies.

Reference	N_s [-]	D_1 [m]	α [deg]	N_b investigated [-]	$N_{b,ott}$ [-]	$N_{b,Mockmore}$ [-]	$N_{b,ott}/N_{b,Mockmore}$ [-]
Khosrowpanah et al. (1988)	51.63	0.304	16	10,15,20	15	18	0.83
Desai and Aziz (1994) [a]	92.90	0.305	22	15,20,25,30	30	23	1.10
Totapally and Aziz (1994)		0.305	22	15,20,25,30,35,40	35	23	1.54
Joshi et al. (1995)	60.50	0.300	16	8,10,16,20,24,30	20	18	1.108
Costa Pereira and Borges (1996)	77.10	0.300	15	10,25	25	18	1.38
Olgun (2000)	91.17	0.170	16	20,24,28,32	24	18	1.33
Acharya et al. (2015)	65.00	0.300	16	16,18,20,22,24,26,28,32	22	18	1.22
Ceballos et al. (2017)	89.42	0.297		16,20,23,25,28,32	28		

[a] = optimal configuration as shown in Anand et al. (2021).

Table 3
Blade thickness from different studies.

Reference	H	Q [m^3/s]	t_b [mm]	t_b/B [-]
Mockmore and Merryfield (1949)	4.87	0.085	3	0.010
Desai and Aziz (1994)	0.5	0.040	3.2	0.021
Joshi et al. (1995)	5	0.072	3	0.009
Fukutomi et al. (1995)	1.48		5.7	0.057
Kokubu et al. (2012)	3.15	0.037	3	0.009
Khan e Badshah (2014)	6	0.175	6.1	0.023
Adhikari (2016)	10	0.105	3.2	0.016
Adhikari (2016)	10	0.105	3.2	0.014
Das et al. (2013)	2	0.120	3	0.006
Acharya et al. (2019)	5	0.010	3	0.033
Ebhota and Tabakov (2021)	13.7	0.5	3–5	0.009–0.115

performance, thus, shaft sizing can be determined based on material strength and respective cost implication (Legonda, 2016).

3.4. Application and additional optimizations

In order to determine the typical Banki dimensions, Table 4 depicts the results of the proposed methodology, assuming $SR_{opt}/SR_{th} = 1.13$ and $B/b = 1$ for the sake of simplicity. If costs are not a significant problem, $B/b = 1.5$ should be used to optimize the efficiency, multiplying by 1.5 the calculated width b. The proposed equation (Fig. 11) generally estimates 32 blades for full scale turbines (Table 4) because the resultant characteristic speed range is very narrow.

The final efficiency can be estimated by the empirical equation of Desai and Aziz (1994):

$$\eta_{max} = 26.7 - 41.11\frac{D_2}{D_1} + 0.86 \cdot N_b + \frac{2,063.53}{\alpha} - 4.16 \cdot \frac{B}{b} + 0.31 \cdot \beta_2 \ [-] \tag{28}$$

Novel optimization strategies have been recently developed to further improve the performance: (1) inner guide to better direct the flow to the second stage (Kokubu et al., 2012; Saini et al., 2022), especially at part load operation; (2) a double-nozzle turbine instead of a single-nozzle (Adhikari and Wood, 2018) to increase the efficiency, reduce vibration, and make easier the part-load control as one nozzle can be closed for low flow rates; (3) a draft tube for counter-pressure operation (Sinagra et al., 2020); (4) Choi et al. (2008) showed that aeration is important to improve the efficiency, as the air layer suppresses collision losses on the shaft and recirculation losses. (5) Rantererung et al. (2020) showed that the horizontal nozzle performed better than the vertical nozzle, while with the double nozzle the highest efficiency could be reached (in a horizontal axis turbine, the vertical nozzle is located above the runner, while the horizontal nozzle is installed laterally). (6) Mitigation of vibrations with cavities in the casing (Otsuka et al., 2022).

4. Materials

The typical used material is the steel. The Italian companies *Italperfo s.r.l.* and *45Engineering* (pers. comm., 2021) suggest the following steel numbers:

- Steel 1.0503 and 1.0038: runner, shaft, blades
- Steel 1.0038 electro-welded for the casing
- Steel 1.0038 for the nozzle
- Inox martensitic steel 1.4057 for the distributor

Ossberger GmbH-Co (pers. comm., 2021) suggests:

- Standard steel for $H_n < 100$ m
- Steel 1.4571 (Inox austentic steel with titanium) for $H_n > 100$ m

Naing et al. (2019) studied an aluminium alloy 6061, finding an almost identical performance to that of steel AISI 1020. Ebhota and Tabakov (2021) used AISI 1045 Steel, cold drawn.

5. Costs

Despite the peak efficiency of Banki turbines is often lower than the efficiency of Kaplan and Francis turbines, their manufacture simplicity and flat efficiency curve under varying conditions make them rather cost-effective. The mechanic system is quite simple so that the construction and maintenance can be performed by local manpower. Costs are generally lower compared to Kaplan or Francis turbines.

Although it is quite difficult to find general indication due to a lack of information in scientific papers or for the natural reluctance of producers to publish prices, some preliminary indications can be given. Acharya et al. (2019) proposed a small Banki turbine (i.e., diameter $D_1 = 0.15$ m, flow 10 l/s, head $H = 5$ m, power $P_{out} = 245$ W) and claims that it is possible to build a prototype with less than 30 €: his scope was to realize a cheap and reliable hydropower system in rural and isolated areas in Nepal. The low cost may be justified by the geographic context and the very low power, used for local and remote purposes.

On the other side, Ott and Chappell (1989, 1991) estimated an actualized cost of 500 €/kW in the construction of a Banki turbine (see also Desai, 1993) with a power of 336 kW. Similar values are reported in some personal communications obtained by the Authors from engineering companies, i.e., 445–497 €/kW for turbines with power of 105–115 kW (excluding the generator and the gearbox), and in Das et al. (2013) that found a value of 441 €/kW. Fig. 12 shows the collected data of another company: the lower is the power, the higher is the cost per

Table 4
Overall dimensions of a Banki turbine, where N_{final} was selected based on the available number of poles of the generator and to satisfy that the ratio D_1/B falls within the range 1–3 ±10%. The number of blades calculated with the equation found in this paper was applied also outside of its range of H_n/D, but respecting the range of N_s. See *Discussion* section.

Number	H_n [m]	Q [m^3/s]	N (Eq. (7)) [rpm]	N (Eq. (24)) [rpm]	N_{chosen} [rpm]	N_s [-]	D_1 [m]	b [m]	H_n/D	N_b	N_b[a]
1	2	0.25	434	160	167	138	0.369	0.376	5		76
2	10	0.5	455	219	231	81	0.595	0.208	17	32	62
3	50	0.5	676	595	750	79	0.409	0.135	122	32	38
4	100	0.5	801	914	1500	93	0.290	0.135	345	28	28
5	100	1	566	670	1000	88	0.434	0.180	230	30	32
6	200	0.5	949	1405	3000	112	0.205	0.135	976		22
7	10	1	322	161	167	83	0.824	0.300	12	32	70
8	25	1	403	284	300	75	0.724	0.216	35	32	52
9	25	2	285	208	214	76	1.013	0.309	25	32	60
10	50	4	239	234	273	81	1.126	0.393	44	32	52
11	50	2	338	320	375	79	0.819	0.270	61	32	48
12	5	2	192	111	115	136	0.842	0.832	6		84
13	10	5	144	113	115	128	1.190	1.040	8		80

[a] = Sammartano et al. (2016).

kW. Equation (29) was found:

$$C = 9.6\, P_{out}^{-0.459} \quad (29)$$

where C is the cost in k€ and P_{out} is expressed in kW.

Costs are also in line with some Italian case studies (Giusti and Beconcini, 2016), where the electro-mechanical cost of 1560 €/kW was found for an installed power of 96 kW, while 828 €/kW for a 374 kW turbine, and the removal cost of the electro-mechanical equipment was quantified in 30,000 € (Studio T.En, 2014). In Celano (2017), the electro-mechanical cost was 1520 €/kW for a 113 kW turbine (80% assumed efficiency), with the other costs amount to 610,000 € (excavation, civil works, penstock, gates and racks, electrical works).

6. Environmental performance

Considering the increasing attention on the environmental impacts of hydropower plants and on fish friendly turbines (Quaranta et al., 2021), it is worth to include here some considerations on the environmental performance of Banki turbines. Dainys et al. (2018) estimated a fish mortality up to 100% in small Banki turbines, while Gloss and Wahl (1983) estimated a fish mortality from 25% to 70% for salmon between 85 mm and 280 mm in body length (two turbines were tested in Gloss and Wahl, 1983, with the following design parameters: external diameter 1 m and 1.25 m, spacing among blades approximately 30 mm, $N =$ 135 and 104 rpm, 650 and 850 kW). The flow, passing through the runner, favors the self-cleaning capacity of the machine by continuously removing the sediments (pers. comm. of Ossberger GmbH-Co, 2021). Adhikari et al. (2016) showed that cavitation was found only in the second stage.

7. Discussion and conclusions

The Banki turbine is a low cost and flexible turbine that can be applied in different geographic areas (see the *Introduction*) and engineering contexts (see Appendix 4), with power output typically below 1 MW. The cost is lower that of Kaplan turbine and the flexibility is higher than that of Francis turbines. Typical full-scale dimensions range from $D_1 = 0.20$ m to $D_1 = 1.4$ m (external diameter), from $B = 0.14$ m to $B =$ 0.90 m (runner width) and rotational speeds from $N = 100$ rpm to $N =$ 3000 rpm.

However, the design methodologies proposed in literature are often not clear: some geometric and kinematic parameters are assumed with no specific criteria and other parameters are selected after experiments or CFD simulations. Some proposed equations are not dimensionless and does not always work well, as also happen with Kaplan and Francis turbines, as highlighted in *Proposed design methodology*.

In this paper, the optimal design parameters are suggested based on literature information, and new equations are proposed to be used in the design of Banki turbines, e.g. the optimal number of blades, rotational speed and speed ratio. Novel data on costs and materials, collected from hydropower companies, are also described and elaborated.

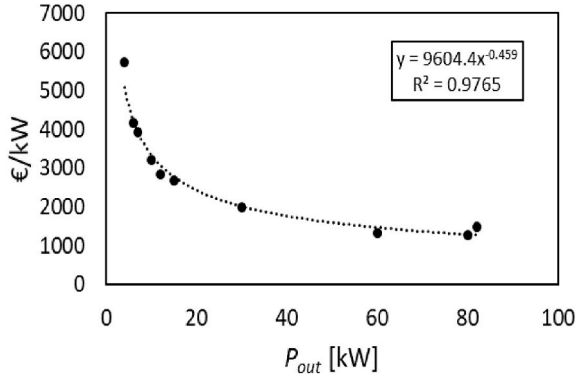

Fig. 12. Cost per kW of a Banki turbine from a European company.

It was found that the optimal number of blades, expressed in dimensionless terms, exhibits a parabolic trend versus the characteristic speed N_s, with a maximum dimensionless value at $N_s = 80$. The proposed equation was achieved interpolating all the available literature data found by the Authors. It is suggested to use the new equation within the range $40 < N_s < 110$ and for $H_n/D < 35$ to respect the used input data. Therefore, this equation complements that of Sammartano et al. (2016) (see Table 1), valid within the range $70 < H_n/D_1 < 120$. However, as shown in Tables 4, $5 < H_n/D < 1000$, so that additional equations should be determined to cover the entire spectrum of the Banki operating range. Nevertheless, these equations were applied to the turbines listed in Table 4, also outside of their H_n/D range, just as a sake of example The number of blades ranges from 28 to 32 with our equation, being hence almost independent on the diameter (see below for the explanation), and from 22 to 84 with Sammartano methodology. Sammartano et al. (2016) estimates a higher value probably because a higher external diameter D_1 was generally adopted (thus more blades are required if a certain blade spacing is chosen), as there were not upper limitations on the ratio D_1/b, and a higher ratio D_1/D_2 (0.75) was used, implying a smaller length of the blades and, therefore, a higher number of blades to better guide the flow. Therefore, in our study it was found that the optimal number of blades depends on the characteristic speed and on β_1 (Fig. 11), while the effects of the diameter could not be studied due to lack of data. Instead, in Sammartano et al. (2016) the optimal number of blades depended on the ratio H_n/D_1 (i.e., on the diameter, that depends on the rotational speed), as also shown in Khan and Badshah (2014) and in Verhaart (1983). More research should be carried out in this context to express the number of blades as a function of both parameters, and to derive other equations for the entire range of operation and dimensions.

For the rotational speed estimation, a new equation was found (Eq. (24)), but with two different coefficients for $N_s < 90$ and $N_s > 90$. Although it is not possible to understand what happens at $N_s = 80$–90 within the aim of this study, further studies should aim at better examining the flow behaviour within this range. It must be noted that the elaborated data refer to literature ones, with maximum power 6 kW (except for 9 turbines, Reihani et al., 2014; pers. comm. Santolin, 2021, Hydrowatt gmbh), and mostly being below 1 kW. Considering the turbines investigated in literature, the average error of the estimated rotational speed by Eq. (24) with respect to the real rotational speed is 12.4%, ranging between 0.1% and 47%, while it is 659% using Eq. (7), because Eq. (7) should be used only for high head turbines. When considering the larger turbines (Appendix 1), the error of Eq. (7) is 62%, while it is 14% using Eq. (24). Looking at Table 4, Eq. (24) and Eq. (7) predict similar values when $H_n > 50$ m, thus Eq. (24) is also valid for high heads.

By elaborating the tip speed ratio of the collected data, it was found that the optimal one is 1.11–1.15 fold higher than the theoretical one (that is 0.5). This means that the turbine must rotate faster than its theoretical speed. This is contrary to what happens with Pelton turbines, where the rotational speed is generally lower than the theoretical one, in order to increase the relative flow velocity to compensate the velocity reduction due to friction. The different behavior may be due to the fact that in Banki turbines the energy is exchanged in two stages, and this may affect the speed ratio more than friction. The turbine rotates faster, thus the relative velocity in the first stage is lower. However, a clear explanation cannot be found within this study, and future studies should investigate the flow field at different speed ratios to answer to this question.

The typical cost of full scale turbines ranges from 1000 €/kW for a 80 kW turbine to 6000 €/kW for a 4 kW turbine, including the generator, which is a typical cost range in the micro hydropower field (i.e., <100 kW). Extrapolating the results to a 1000 kW turbine, the cost is estimated in 403 €/kW, but that has to be verified with real data, since this extrapolation may not be accurate (the presented results are within the

range 4–80 kW). The cost of micro Banki turbines can be noticeably lower in low income countries. It was also shown as the impact on fish is high and the turbine cannot be classified as fish-friendly turbine. This is an obvious result, considering the high flow velocity and the working behaviour of the Banki turbine.

Furthermore, full scale turbines should be analysed and their behaviour better investigated, since literature studies generally refer to turbine below 6 kW, and mostly being below 1 kW. Only few studies refer to full scale turbines (e.g., Reihani et al., 2014; Obretenov and Tsalov, 2021). More light should be done on the optimal ratio D_1/B and on how it affects flow behaviour and efficiency. More efforts should also be spent on the optimal design of the casing, since it affects different aspects of the operation, e.g. aeration, multiphase flow behaviour and vibrations, as in Pelton turbines (Quaranta and Trivedi, 2021).

Declaration of competing interest

The authors declare that they have no known competing financial interests or personal relationships that could have appeared to influence the work reported in this paper.

Acknowledgements

The Authors want to thank the following companies for their input: 45 Engineering (Alberto Santolin), Ossberger GmbH-Co, Italperfo and IREM. Some data from the website of Hydrowatt gmbh are included in Appendix 1. Thanks also to Markus Wirth of Voith Hydro for the information on the installed Banki turbines in the EU28. The open access fee was paid by the European Commission Joint Research Centre.

Appendix 1. Investigated turbines to estimate the optimal rotational speed

Reference	Q [m^3/s]	H [m]	N_{real} [rpm]	N_s [-]	N^* [-]	Q^* [-]	N [1] [rpm]
Khosrowpanah et al. (1988)	0.02	0.94	290	105.95	63.509	0.005	217.08
	0.02	0.56	225	131.54	38.032	0.019	157.46
	0.02	0.396	183	144.78	26.012	0.046	127.01
	0.024	1.454	356	95.87	96.963	0.002	262.18
	0.024	0.908	290	119.12	62.418	0.007	195.8
	0.024	0.686	240	126.46	44.900	0.014	164.56
	0.029	1.31	350	112.03	90.485	0.003	225.79
	0.029	0.991	300	124.79	67.457	0.007	189.91
	0.029	1.22	165	63.43	41.166	0.004	216.04
	0.029	0.588	115	78.58	19.919	0.025	137.4
	0.029	0.335	87	94.26	11.374	0.101	96.94
	0.033	1.64	190	59.21	54.960	0.002	244.94
	0.033	0.854	138	71.8	28.806	0.011	163.44
	0.033	0.448	100	88.78	15.119	0.055	109.56
	0.04	2.604	240	54.39	87.479	0.001	299.31
	0.04	1.281	170	68.51	43.461	0.005	192.8
	0.04	0.744	130	82.58	25.328	0.019	137.66
	0.029	1.329	175	62.18	45.569	0.003	227.81
	0.029	0.61	120	79.77	21.170	0.023	140.57
	0.029	0.341	90	95.61	11.871	0.096	98.02
	0.033	2.196	220	54.19	73.639	0.001	293.53
	0.033	0.972	149	70.36	33.181	0.008	177.09
	0.033	0.603	120	83.48	21.048	0.026	131.72
	0.04	1.247	170	70.48	42.880	0.005	189.61
	0.04	0.732	130	83.6	25.123	0.02	136.27
	0.04	1.894	210	59.32	65.280	0.002	245.69
	0.04	0.756	130	78.45	25.531	0.018	139.03
	0.04	0.436	104	96.37	15.511	0.072	98.83
	0.043	2.315	232	57.34	79.733	0.001	269.38
	0.043	0.967	150	74.76	33.318	0.011	156.79
	0.043	0.542	114	90.79	18.957	0.045	109.5
Adhikari and Wood (2018)	0.02	1.337	200	66.07	52.21	0.002	270.27
	0.03	1.337	200	81.85	52.21	0.003	225.38
	0.04	1.337	200	95.05	52.21	0.004	198.13
Sammartano et al. (2013)	0.06	10	757	95.78	540.714	0.00004	574.82
Galvis-Holguin et al. (2021)	0.0162	0.5	160	97.73	25.555	0.021	161.3
pers. comm. Santolin, 2021	0.644	19.95	429	10.22	432.813	0.00008	304.6
	0.48	30.52	375	5.61	467.946	0.00002	452.26
Reihani et al. (2014)	0.20	60	1000	58.11	1749	0.00000162	961
Hydrowatt gmbh	1.8	5.7	156	158.43	84.13	0.005241521	87
Hydrowatt gmbh	0.5	3.5	181	128.22	76.49	0.004928013	114
Hydrowatt gmbh	0.7	6.3	241	127.77	136.63	0.001587152	141
Hydrowatt gmbh	1.5	2.2	80	149.29	26.80	0.047196144	53
Hydrowatt gmbh	0.5	4.5	246	159.24	117.87	0.002629122	133
Hydrowatt gmbh	0.2	4.8	266	105.89	131.64	0.00089495	208
Studio T.En (2014)	3.0	14	189	127	159.7	0.00092	120

[1]The estimated rotational speed N included in this table should then be multiplied by the correction factors 1.35 and 0.93 when $N_s > 90$ or $N_s < 90$, respectively.

Appendix 2. Investigated turbines to estimate the optimal tip speed ratio

Reference	α [deg]	N_s [-]	SR_{opt} [-]	SR_{th} [-]	SR_{opt}/SR_{th} [-]
Khosrowpanah et al. (1988)	16	105.95	0.53	0.4806	1.1027
	16	131.54	0.54	0.4806	1.1235
	16	144.78	0.53	0.4806	1.1027
	16	95.87	0.53	0.4806	1.1027
	16	119.12	0.54	0.4806	1.1235
	16	126.46	0.53	0.4806	1.1027
	16	112.03	0.54	0.4806	1.1235
	16	124.79	0.54	0.4806	1.1235
	16	63.43	0.53	0.4806	1.1027
	16	78.58	0.54	0.4806	1.1235
	16	94.26	0.54	0.4806	1.1235
	16	59.21	0.53	0.4806	1.1027
	16	71.80	0.54	0.4806	1.1235
	16	88.78	0.54	0.4806	1.1235
	16	54.39	0.53	0.4806	1.1027
	16	68.51	0.54	0.4806	1.1235
	16	82.58	0.54	0.4806	1.1235
	16	62.18	0.54	0.4806	1.1235
	16	79.77	0.55	0.4806	1.1443
	16	95.61	0.55	0.4806	1.1443
	16	54.19	0.53	0.4806	1.1027
	16	70.36	0.54	0.4806	1.1235
	16	83.48	0.55	0.4806	1.1443
	16	70.48	0.54	0.4806	1.1235
	16	83.60	0.54	0.4806	1.1235
	16	59.32	0.55	0.4806	1.1443
	16	78.45	0.54	0.4806	1.1235
	16	96.37	0.55	0.4806	1.1443
	16	57.34	0.55	0.4806	1.1443
	16	74.76	0.55	0.4806	1.1443
	16	90.79	0.55	0.4806	1.1443
Adhikari and Wood (2018)	22	64.88	0.616	0.4636	1.3288
	22	80.38	0.616	0.4636	1.3288
	22	93.34	0.616	0.4636	1.3288
Sammartano et al. (2013)	22	95.78	0.509	0.4636	1.0979
Fiuzat and Akerkar (1989)	22		0.5	0.4636	1.0785
	22		0.5	0.4636	1.0785
Galvis-Holguin et al. (2021)	22	97.73	0.545	0.4636	1.1756
Costa Pereira and Borges (1996)	13		0.454	0.4872	0.9319

Appendix 3. Investigated turbines to estimate the optimal shape ratio

Reference	H [m]	Q [m^3/s]	N [rpm]	N_s [-]	η [%]	D_1 [m]	B [m]	b [m]	D_1/B	D_1/b
Mockmore and Merryfield (1949)	4.87	0.085	263	60.41	68.0	0.333	0.305	0.305	1.09	1.09
Khosrowpanah et al. (1988)	1.79	0.030	176	51.63	70.0	0.304	0.152	0.152	2.00	2.00
Desai and Aziz (1994)[1]	0.5	0.040	94	92.90	88.0	0.461	0.152	0.101	3.03	4.55
Totapally and Aziz (1994)					92.0	0.305	0.152	0.102	2.01	3.00
Joshi et al. (1995)	5	0.072	298	60.50	64.8	0.300	0.325	0.300	0.92	1.00
Costa Pereira and Borges (1996)	3	0.080	231	77.10	73.8	0.300	0.215	0.210	1.40	1.43
Olgun (2000)	15	0.082	911	91.17	72.0	0.170	0.145	0.150	1.17	1.13
Chen and Choi (2013)	20	0.465	526	107.13	81.3	0.340	0.500	0.500	0.68	0.68
Sinagra et al. (2014)	12	0.620	360	124.74	82.1	0.385	0.530		0.73	
Fukutomi et al. (1995)	1.48		154			0.315	0.100	0.100	3.15	3.15
De Andrade et al. (2011)	35	0.135	805	55.75	75.0	0.294	0.150	0.150	1.96	1.96
Kokubu et al. (2012)	3.15	0.037	284	57.53	62.9	0.250				
Khan and Badshah (2014)	6	0.175	261	68.28	58.5	0.350	0.271		1.29	
Adhikari (2016)	10	0.105	400	68.92	91.0	0.316	0.150	0.150	2.11	2.11
Adhikari (2016)	10	0.105	400	60.01	69.0	0.305	0.102	0.102	2.99	2.99
Chattha et al. (2014)	4.9	0.100	221	62.45	88.0	0.400	0.591	0.396	0.68	1.01
Sirojuddin, Wardhana et al.,. (2020)	5.5	0.033	469	71.43	92.4	0.200	0.200		1.00	
Das et al. (2013)	2	0.120	120	59.64	59.0	0.470	0.470	0.440	1.00	1.07
Acharya et al. (2019)	5	0.018	596	52.99	50.0	0.150	0.090		1.67	
Acharya et al. (2015)	10	0.100	642	98.95	76.6	0.200				
Ceballos et al. (2017)	10	0.148	450	89.42	86.0					
Khosrowpanah et al. (1988)	0.94	0.020	290	105.95	62	0.152	0.152		1.00	
	0.56	0.020	225	131.54	73	0.152	0.152		1.00	
	0.40	0.020	183	144.78	79.5	0.152	0.152		1.00	
	1.45	0.024	356	95.87	54	0.152	0.152		1.00	
	0.91	0.024	290	119.12	62	0.152	0.152		1.00	
	0.69	0.024	240	126.46	67	0.152	0.152		1.00	
	1.31	0.029	350	112.03	54	0.152	0.152		1.00	
	0.99	0.029	300	124.79	60	0.152	0.152		1.00	
	1.22	0.029	165	63.43	70	0.305	0.152		2.01	

(continued on next page)

(*continued*)

Reference	H [m]	Q [m^3/s]	N [rpm]	N_s [-]	η [%]	D_1 [m]	B [m]	b [m]	D_1/B	D_1/b
	0.59	0.029	115	78.58	74	0.305	0.152		2.01	
	0.34	0.029	87	94.26	80	0.305	0.152		2.01	
	1.64	0.033	190	59.21	63	0.305	0.152		2.01	
	0.85	0.033	138	71.80	66	0.305	0.152		2.01	
	0.45	0.033	100	88.78	73	0.305	0.152		2.01	
	2.60	0.040	240	54.39	55	0.305	0.152		2.01	
	1.28	0.040	170	68.51	60	0.305	0.152		2.01	
	0.74	0.040	130	82.58	66	0.305	0.152		2.01	
	1.33	0.029	175	62.18	68	0.305	0.152		2.01	
	0.61	0.029	120	79.77	74	0.305	0.152		2.01	
	0.34	0.029	90	95.61	79	0.305	0.152		2.01	
	2.20	0.033	220	54.19	61	0.305	0.152		2.01	
	0.97	0.033	149	70.36	66	0.305	0.152		2.01	
	0.60	0.033	120	83.48	70	0.305	0.152		2.01	
	1.25	0.040	170	70.48	61	0.305	0.152		2.01	
	0.73	0.040	130	83.60	66	0.305	0.152		2.01	
	1.89	0.040	210	59.32	53	0.305	0.152		2.01	
	0.76	0.040	130	78.45	61	0.305	0.152		2.01	
	0.44	0.040	104	96.37	63	0.305	0.152		2.01	
	2.32	0.043	232	57.34	51	0.305	0.152		2.01	
	0.97	0.043	150	74.76	56	0.305	0.152		2.01	
	0.54	0.043	114	90.79	60	0.305	0.152		2.01	
Adhikari and Wood (2018)	1.37	0.020	200	64.88	86	0.305	0.1016	0.102	3.00	3.00
	1.37	0.030	200	80.38	88	0.305	0.1016	0.102	3.00	3.00
	1.37	0.040	200	93.34	89	0.305	0.1016	0.102	3.00	3.00
Sammartano et al. (2013)	10.00	0.060	757	95.78	86	0.161	0.139	0.093	1.16	1.73
Fiuzat and Akerkar (1989)					78.8	0.3048	0.152	0.152	2.01	2.01
					72.2	0.3048	0.152	0.152	2.01	2.01
Galvis-Holguin et al. (2021)	0.50	0.016	160	97.73	83	0.200		0		
Costa Pereira and Borges (2017)	3.10			0.00	84.8	0.300	0.215	0.21	1.40	1.43
	4.30			0.00	84.8	0.300	0.215	0.21	1.40	1.43
	5.00			0.00	84.8	0.300	0.215	0.21	1.40	1.43

[1] optimal configuration as shown in Anand et al. (2021).

Appendix 4

Further applications

Similar designs of the Banki turbine can be used in different contexts outside of traditional hydropower schemes:

1) Banki turbines can be used as Power Recovery System (PRS) in place of hydro valves for discharge and pressure regulation (see for example Sammartano et al., 2017; Sinagra et al., 2020; Sinagra et al., 2021). In this way it is possible to harvest renewable energy from water distribution networks without the loosing of functionality (i.e., discharge and pressure regulation), which is an emerging trend, especially in Europe (Quaranta et al., 2022). In this context, a counter-pressure operation is generally adopted, with a draft tube downstream.
2) Similar-Banki turbine can be a promising source of electricity when, in existing small dams, it is necessary to install a hydropower plant without interventions on the dam, and installing a set of Banki turbines at the dam toe, and exploiting the flow flowing along the downstream facing of the dam (e.g., Clark, 2020). In this case, the turbine can work similarly to an undershot water wheel, Poncelet type (Quaranta and Revelli, 2018).
3) Shikama et al. (2021) investigated the performance of a waterfall-type crossflow hydraulic turbines via experimental and numerical simulation. They found that the efficiency of waterfall-type crossflow hydraulic turbine can be higher than the corresponding underflow type (see also Nishi et al., 2014; Nishi et al., 2014b).
4) Prasad et al. (2014) and Kang et al. (2022) studied the Banki turbine as hydraulic converter for wave energy applications.
5) Several Authors (e.g., Tian et al., 2017a, 2017b; Bani-Hani et al., 2018; Matias et al., 2021) propose a similar-Banki type Vertical Axis Wind Turbine (VAWT) to exploit the wind energy in highways caused by the passing vehicles. Bani-Hani et al. (2018) presented an experimental study on a prototype that can produce 48 W of power (efficiency 34.6%) suitable for lights or traffic signals. Using a CFD simulation Tian et al. (2017a, 2017b) studied the performance of a VAWT with respect the car velocity and the position of the turbine. They also showed how a power up to 139.60 W can be reached from the wakes generated by vehicles on the passing lane. To improve the performance, Matias et al. (2021) showed how the position of a windshield can change the energy captured by the VAWT: when a car model is used, the increase can be up to 16.14% with respect a no windshield case; on the contrary, when a bus model is implemented, they found a decrease by 64.77%.

References

Acharya, N., Kim, C.G., Thapa, B., Lee, Y.H., 2015. Numerical analysis and performance enhancement of a crossflow hydro turbine. Renew. Energy 80, 819–826.

Acharya, B., Jalswal, N., Kausal, K.C., 2019. Design and Fabrication of Crossflow Turbine for Rural Areas. Kathmandu University, student report.

Achebe, C.H., Okafor, O.C., Obika, E.N., 2020. Design and implementation of a crossflow turbine for Pico hydropower electricity generation. Heliyon 6, e04523.

Adhikari, R., 2016. Design Improvement of Crossflow Hydro Turbine. Ph.D. Thesis. University of Calgary, Calgary, AB, Canada.

Adhikari, R.C., Vaz, J., Wood, D., 2016. Cavitation inception in crossflow hydro turbines. Energies 9, 237.

Adhikari, R.C., Wood, D.H., 2018. Computational analysis of part-load flow control for crossflow hydro-turbines. Energy Sustain. Dev. 45, 38–45.

Anand, R.S., Jawahar, C.P., Bellos, E., Malmquist, A., 2021. A comprehensive review on Crossflow turbine for hydropower applications. Ocean. Eng. 240, 110015.

Bani-Hani, E.H., Sedaghat, A., Al-Shemmary, M., Hussain, A., Alshaieb, A., Kakoli, H., 2018. Feasibility of highway energy harvesting using a vertical Axis wind turbine. Energy Eng. J. Assoc. Energy Eng. 115, 61–74.

Ceballos, Y.C., Valencia, M.C., Zuluaga, D.H., Del Rio, J.S., García, S.V., 2017. Influence of the number of blades in the power generated by a Michell Banki Turbine. Renew. Energy Res. IJRER 7 (4), 1989, 199.
Celano, 2017. Progetto di un impianto idroelettrico sul torrente Cogliandrino con Pc<250 kW. Relazione Tecnica.
Cesoniene, L., Dapkiene, M., Punys, P., 2020. Assessment of the impact of small hydropower plants on the ecological status indicators of water bodies: a case study in Lithuania. Water 13, 433.
Chattha, J.A., Khan, M.S., Iftekhar, H., Shahid, S., 2014. Standardization of cross-flow turbine design for typical micro-hydro site conditions in Pakistan. In: ASME Power Conference, p. 32049.
Chen, Z.M., Choi, Y.D., 2013. Performance and internal flow characteristics of a cross-flow turbine by guide vane angle. IOP Conf. Ser. Mater. Sci. Eng. 52 (5), 052031.
Choi, Y.D., Lim, J.I., Kim, Y.T., Lee, Y.H., 2008. Performance and internal flow characteristics of a cross-flow hydro turbine by the shapes of nozzle and runner blade. J. Fluid Sci. Technol. 3 (3), 398–409.
Clark, A.M., 2020. Computation Analysis of Nozzle Designs for a Novel Low Head Hydroturbine. Ohio State University, Thesis.
Costa Pereira, N.H., Borges, J.E., 1996. Study of the nozzle flow in a cross-flow turbine. Mech. Sci. 38 (3), 283–302.
Costa Pereira, N.H., Borges, J.E., 2017. Prediction of the cross-flow turbine efficiency with experimental verification. Hydraul. Eng. 143 (1), 04016075.
Dainys, J., Stakėnas, S., Gorfine, H., Ložys, L., 2018. Mortality of silver eels migrating through different types of hydropower turbines in Lithuania. River Res. Appl. 34 (1), 52–59.
Das, N.K., Islam, M.T., Basher, E., 2013. Design and fabrication of a cost effective cross flow hydro turbine for low head micro hydro power system. Int. Conf. Mech. Eng. Renew. Energy ICMERE2013. PI-147.
De Andrade, J., Curiel, C., Kenyery, F., Aguillón, O., Vásquez, A., Asuaje, M., 2011. Numerical investigation of the internal flow in a Banki turbine. Rotating Mach. 841214.
Desai, V.R., Aziz, N.M., 1994. Parametric evaluation of cross-flow turbine performance. Energy Eng. J. Assoc. Energy Eng. 120, 17–34.
Desai, V.R., 1993. Ph.D. Thesis. A Parametric Study of Cross-Flow Turbine Performances, 932S87S. Clemson University.
Durali, M., 1976. Design of small water turbines for farms and small communities. Dep. Mech. Eng. Master Sci. Doctoral Dissertation.
Ebhota, W.S., Tabakov, P.Y., 2021. Design process sequence of crossflow turbine system and the evaluation of structural integrity factors. Energy Environ. Eng. 1–17.
Fiuzat, A., Akerkar, B., 1989. The use of interior guide tube in cross flow turbines. Waterpower 1111–1119. ASCE.
Fukutomi, J., Nakase, Y., Ichimiya, M., Ebisu, H., 1995. Unsteady fluid forces on a blade in a cross-flow turbine. JSME Int. J. Ser. B Fluids Therm. Eng. 38 (3), 404–410.
Galvis-Holguin, S., Sierra-Del-Rio, J., Hincapié-Zuluaga, D., Chica-Arrieta, E., 2021. Numerical Validation of a Design Methodology for Cross-Flow Type Michel-Banki. Instituto Mexicano de Tecnologia del Agua.
Giusti, M., Beconcini, C., 2016. Studio di fattibilità per la realizzazione di un impianto idroelettrico presso l'acquedotto idropotabile di Massa Centro.
Gloss, S.P., Wahl, J.R., 1983. Mortality of juvenile salmonids passing through ossberger crossflow turbines at small-scale hydroelectric sites. Trans. Am. Fish. Soc. 112 (2A).
Hannachi, M., Ketata, A., Sinagra, M., Aricò, C., Tucciarelli, T., Driss, Z., 2021. A novel pressure regulation system based on Banki hydro turbine for energy recovery under in-range and out-range discharge conditions. Energy Convers. Manag. 243, 114417.
Ho-Yan, B., Lubitz, W.D., 2011. Performance Evaluation of Cross-Flow Turbine for Low Head Application. World Renewable Energy Congress, Sweden.
International Energy Agency (IEA), 2021. Hydropower Special Market Report Analysis and Forecast to 2030.
Joshi, C.B., Seshadri, V., Singh, S.N., 1995. Parametric study on performance of cross-flow turbine. ASCE J. Energy Eng. 121.
Kang, H.G., Lee, Y.H., Kim, C.J., Kang, H.D., 2022. Design optimization of a cross-flow air turbine for an oscillating water column wave energy converter. Energies 15 (7), 2444.
Khan, M.A., Badshah, S., 2014. Design and analysis of cross flow turbine for micro hydro power application using sewerage water. Res. J. Appl. Sci. Eng. Technol. 8 (7), 821–828.
Khosrowpanah, S., Fiuzat, A.A., Albertson, M.L., 1988. Experimental study of cross-flow turbine. Hydraul. Eng. 114 (3), 299–314.
Kokubu, K., Yamasaki, K., Honda, H., Kanemoto, T., 2012. Effect of inner guide on performances of cross flow turbine. IOP Conf. Ser. Earth Environ. Sci. 15 (4), 042035. IOP Publishing.
Legonda, I.A., 2016. An investigation on the flow characteristics in the cross-flow turbine-T15 300. Power Energy Eng. 4, 52–60.
Matias, I.J.T., Danao, L.A.M., Abuam, B.E., 2021. Numerical investigation on the effect of varying the arc lenght of a windshield on the performance of highway installed Banki wind turbine. Fluids 6, 285.
Mehr, G., Durali, M., Khakrand, M.H., Hoghooghi, H., 2019. Use of Successive Numerical Simulations to Design and Optimize the Performance of High-Efficiency Hydraulic Cross-Flow Turbines. *arXiv*-1702.
Michell, A.G.M., 1903. Impulse turbine, n. 760, 898.
Mockmore, C.A., Merryfield, F., 1949. The Banki Water Turbine, Bulletin Series No.25. Engineering Experiment Station, Oregon State College.
Mtalo, F., Wakati, R., Towo, A., Makhanu, S.K., Munyaneza, O., Abate, B., 2010. Design and Fabrication of Cross Flow Turbine. Nile Basin Capacity Building Network.
Naing, K.S.S., Thwe, M.M., Aung, A., 2019. Analysis of structural behaviors on cross-flow turbine runner blade with two different materials. Sci. Eng. Technol. Res. 8, 535–539.
Nasir, B.A., 2013. Design of high efficiency cross-flow turbine for hydro-power plant. Eng. Adv. Technol. 2 (3).
Ngoma, D.H., Wang, Y., Roskilly, T., 2019. Crossflow turbine design specifications for hhaynu micro-hydropower plant-mbulu, Tanzania. Innov. Energy Res. 8 (225), 2.
Nishi, Y., Inagaki, T., Li, Y., Hatano, K., Omiya, R., 2014. Research on the flow field of undershot cross-flow water turbines using experiments and numerical analysis. 27th IAHR Symp. Hydraul. Mach. Syst., 062006
Nishi, Y., Inagaki, T., Li, Y., Omiya, R., Fukutomi, J., 2014b. Study on an undershot cross-flow water turbine. Therm. Sci. 23 (3), 239–245.
Niyonzima, J.B., 2020. Etude du potentiel hydroélectrique de la province Kayanza (Burundi): Application de la turbine Banki-Michell dans l'électrification des zones rurales.
Obretenov, V., Tsalov, T., 2021. Research and design of cross flow water turbines for small HPP. In: E3S Web of Conferences, vol. 320. EDP Sciences, 04007.
Okot, D.K., 2013. Review of small hydropower technology. Renew. Sustain. Energy Rev. 26, 515–520.
Olgun, H., 2000. Effect of interior guide tubes in cross-flow turbine runner on turbine performance. Energy Res. 24, 953–964.
Otsuka, K., Ogawa, N., Iio, S., Kitahora, T., Choi, Y.D., Inagaki, M., 2022. Characteristics and suppression of vibration in cross-flow turbine with a cavity. J. Phys. Conf. 2217 (1), 012063. IOP Publishing.
Ott, R.F., Chappell, J.R., 1989. Design and efficiency testing of a cross-flow turbine. In: Waterpower '89. (Niagara Falls, NY, August 1989), vol. 3, p. 1534.
Ott, R.F., Chappell, J.R., 1991. The crossflow turbine at arbuckle mountain: blending the old with the new. Hydro Rev. 12.
Penche, C., 1998. Layman's Guide Book on How to Develop a Small Hydro Site, second ed. ESHA, Belgium.
Perez-Rodriguez, A.J., Sierra-Del Rio, J., Grisales, L.F., Galvis, S., 2021. Optimization of the efficiency of a michell-banki turbine through the variation of its geometrical parameters using a PSO algotihm. WSEAS Trans. Appl. Theor. Mech. 16, 37–46.
Picone, C., Sinagra, M., Aricò, C., Tucciarelli, T., 2021. Numerical analysis of a new cross-flow type hydraulic turbine for high head and low flow rate. Eng. Appl. Comp. Fluid Mech. 15 (1), 1491–1507.
Prasad, D.D., Ahmed, M.R., Lee, Y.H., 2014. Flow and performance characteristics of a direct drive turbine for wave power generation. Ocean. Eng. 81, 39–49.
Quaranta, E., Revelli, R., 2017. Hydraulic behavior and performance of breastshot water wheels for different numbers of blades. Hydraul. Eng. 13 (1).
Quaranta, E., 2019. Optimal rotational speed of Kaplan and Francis turbines with focus on low-head hydropower applications and dataset collection. Hydraul. Eng. 145 (12), 04019043.
Quaranta, E., Revelli, R., 2018. Gravity water wheels as a micro hydropower energy source: a review based on historic data, design methods, efficiencies and modern optimizations. Renew. Sustain. Energy Rev. 97, 414–427.
Quaranta, E., Hendrick, P., 2020. Rotational speed estimation of Deriaz turbines: trends and dataset collection. In: IAHR Online Conference.
Quaranta, E., Bonjean, M., Cuvato, D., Nicolet, C., Dreyer, M., Gaspoz, A., et al., 2020. Hydropower case study collection: innovative low head and ecologically improved turbines, hydropower in existing infrastructures, hydropeaking reduction, digitalization and governing systems. Sustainability 12 (21), 8873.
Quaranta, E., Pérez-Díaz, J.I., Romero–Gomez, P., Pistocchi, A., 2021. Environmentally enhanced turbines for hydropower plants: current technology and future perspective. Front. Energy Res. 592.
Quaranta, E., Trivedi, C., 2021. The state-of-art of design and research for Pelton turbine casing, weight estimation, counterpressure operation and scientific challenges. Heliyon 7 (12), e08527.
Quaranta, E., Bódis, K., Kasiulis, E., McNabola, A., Pistocchi, A., 2022. Is there a residual and hidden potential for small and micro hydropower in Europe? A screening-level regional assessment. Water Resour. Manag. 36 (6), 1745–1762.
Reihani, A., Ojaghi, A., Derakhshan, S., Beigzadeh, B., 2014. Shaft fatigue life and efficiency improvement of a micro cross flow turbine. Eng. Solid Mech. 2 (1), 1–14.
Rantererung, C.L., Soeparman, S., Soenoko, R., Wahyudi, S., 2020. A double nozzle cross flow turbine fluid flow dynamics. Southwest Jiaot. Univ. 55 (4).
Restrepo, J.D.P., 2014. Study of the Effect of the Geometrical Parameters of the Runner and Operation Conditions on Performance and Flow Characteristics in a Cross Flow Turbine. Thesis. Universidad Eafit Department of Mechanical Engineering.
Saini, G., Saini, R.P., Singal, S.K., 2022. Numerical investigations on performance improvement of cross flow hydro turbine having guide vane mechanism. Energy Sources, Part A Recovery, Util. Environ. Eff. 44 (1), 771–795.
Sammartano, V., Aricò, C., Carravetta, A., Fecarotta, O., Tucciarelli, T., 2013. Banki-michell optimal design by computational fluid dynamics testing and hydrodynamic analysis. Energies 6, 2362–2385.
Sammartano, V., Sinagra, M., Filianoti, P., Tucciarelli, T., 2017. A Banki-Michell turbine for in-line water supply systems. Hydraul. Res. 55 (5), 686–694.
Sammartano, V., Morreale, G., Sinagra, M., Tucciarelli, T., 2016. Numerical and experimental investigation of a cross-flow water turbine. Hydraul. Res. 54 (3), 321–331.
San, M., Nyi, N., 2018. Design of cross flow turbine and analysis of runner's dimensions on various head and flow rate. Sci. Res. Publ. 8 (8), 586–592.
Shikama, H., Wang, T., Yamagata, T., Fujisawa, N., 2021. Experimental and numerical studies on the performance of a waterfall-type cross-flow hydraulic turbine. Energy Sustain. Dev. 64, 128–138.
Sinagra, M., Sammartano, V., Aricò, C., Collura, A., Tucciarelli, T., 2014. Cross-flow turbine design for variable operating conditions. 12th international conference on computing and control for the water industry. Procedia Eng. 70, 1539–1548.

Sinagra, M., Aricò, C., Tucciarelli, T., Morreale, G., 2020. Experimental and numerical analysis of a backpressure Banki inline turbine for pressure regulation and energy production. Renew. Energy 149, 980–986.
Sinagra, M., Picone, C., Aricò, C., Pantano, A., Tucciarelli, T., Hannachi, M., Driss, Z., 2021. Runner optimization in crossflow hydraulic turbines. Water 13 (3), 313.
Spänhoff, B., 2014. Current status and future prospects of hydropower in Saxony (Germany) compared to trends in Germany, the European Union and the World. Renew. Sustain. Energy Rev. 30, 518–525.
Studio T.En, 2014. Centrale idroelettrica denominata Savoniero sul torrente Dragone, Studio di Impatto Ambientale.
Tian, W., Mao, Z., An, X., Zhang, B., Wen, H., 2017b. Numerical study of energy recovery from the wakes of moving vehicles on highways by using a vertical Axis wind turbine. Energy 141, 715–728.
Tian, W., Mao, Z., Li, Y., 2017a. Numerical simulations of a VAWT in the wake of a moving car. Energies 10, 478.
Totapally, H.G.S., Aziz, N.M., 1994. Refinement of cross-flow turbine design parameters. Energy Eng. J. Assoc. Energy Eng. 120 (3).
Verhaart, P., 1983. Blade calculations for water turbines of the Banki type. (EUT report. WPS, Vakgr. warmte-, proces- en stromingstechniek; Vol. WPS3-83.03.R351). Technische Hogeschool Eindhoven.
Win, Z.N.T., Win, H.H., Thein, M., 2016. Design, construction and performance test of cross-flow turbine. Mech. Prod. Eng. 4 (12).
Woldermariam, E.T., Lemu, H.G., 2019. Numerical simulation-based effect characterization and design optimization of a micro cross-flow turbine. Mech. Eng. 65.